

Giardia purification from fecal samples using rigid spiral inertial microfluidics

Cite as: Biomicrofluidics **16**, 014105 (2022); <https://doi.org/10.1063/5.0069406>

Submitted: 31 August 2021 • Accepted: 03 February 2022 • Published Online: 24 February 2022

Lin Ding,  Sajad Razavi Bazaz, Timothy Hall, et al.



View Online



Export Citation



CrossMark

ARTICLES YOU MAY BE INTERESTED IN

Deep learning assisted mechanotyping of individual cells through repeated deformations and relaxations in undulating channels

Biomicrofluidics **16**, 014104 (2022); <https://doi.org/10.1063/5.0077432>

A simple acoustofluidic device for on-chip fabrication of PLGA nanoparticles

Biomicrofluidics **16**, 014103 (2022); <https://doi.org/10.1063/5.0081769>

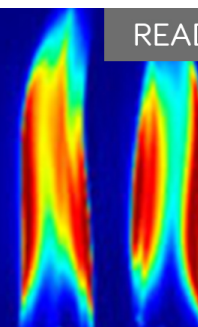
A perspective on magnetic microfluidics: Towards an intelligent future

Biomicrofluidics **16**, 011301 (2022); <https://doi.org/10.1063/5.0079464>

AIP Advances

Fluids and Plasmas Collection

READ NOW



Giardia purification from fecal samples using rigid spiral inertial microfluidics

Cite as: Biomicrofluidics 16, 014105 (2022); doi: 10.1063/5.0069406

Submitted: 31 August 2021 · Accepted: 3 February 2022 ·

Published Online: 24 February 2022



Lin Ding,¹ Sajad Razavi Bazaz,¹ Timothy Hall,² Graham Vesey,² and Majid Ebrahimi Warkiani^{1,3,a)}

AFFILIATIONS

¹School of Biomedical Engineering, University of Technology Sydney, Sydney, New South Wales 2007, Australia

²BioPoint Pty. Ltd, Sydney, NSW 2113, Australia

³Institute of Molecular Medicine, Sechenov University, Moscow 119991, Russia

^{a)}Author to whom correspondence should be addressed: majid.warkiani@uts.edu.au

ABSTRACT

Giardia is one of the most common waterborne pathogens causing around 200×10^6 diarrheal infections annually. It is of great interest to microbiological research as it is among the oldest known eukaryotic cells. Purifying *Giardia* from fecal samples for both research and diagnostic purposes presents one of the most difficult challenges. Traditional purification methods rely on density gradient centrifugation, membrane-based filtration, and sedimentation methods, which suffer from low recovery rates, high costs, and poor efficiency. Here, we report on the use of microfluidics to purify *Giardia* cysts from mouse feces. We propose a rigid spiral microfluidic device with a trapezoidal cross section to effectively separate *Giardia* from surrounding debris. Our characterizations reveal that the recovery rate is concentration-dependent, and our proposed device can achieve recovery rates as high as 75% with 0.75 ml/min throughput. Moreover, this device can purify *Giardia* from extremely turbid samples to a level where cysts are visually distinguishable with just one round of purification. This highly scalable and versatile 3D printed microfluidic device is then capable of further purifying or enhancing the recovery rate of the samples by recirculation. This device also has the potential to purify other gastrointestinal pathogens of similar size, and throughput can be significantly increased by parallelization.

Published under an exclusive license by AIP Publishing. <https://doi.org/10.1063/5.0069406>

I. INTRODUCTION

Giardia is one of the most common gastrointestinal pathogens globally and is one of the oldest divergent eukaryotes.¹ It causes $\sim 200 \times 10^6$ diarrheal, abdominal cramping, and intestinal malabsorption cases annually,² and chronic infection has been found to be highly related to growth retardation in children in developing countries.³ Identifying the presence of *Giardia* and its cyst in fecal samples is currently the gold standard for infection diagnosis, and purifying *Giardia* from feces of infected animals is the most common way of obtaining *Giardia* for research purposes.⁴ As such, there is a continual demand for the purification of *Giardia* from feces; however, existing methods of purification present some major challenges.

Fecal samples generally contain high concentrations of micro-debris with sizes ranging from 1 to $300 \mu\text{m}$. These microparticles can include mucus, lipids, bacteria, insects, protein aggregates, dust,^{5,6} and sometimes large, undigested food particles like sweet corn. As it is often challenging to distinguish cysts from these contaminants, *Giardia* is considered one of the most “misdiagnosed,

undiagnosed, or over-diagnosed parasites.”⁷ The most common method of *Giardia* identification is microscopy; however, it is often inaccurate and prone to human error.⁶ Methods of purifying *Giardia* from fecal samples include density gradient centrifugation,¹ membrane-based filtration, gravity sedimentation, and flocculation.^{6,8} Each of these techniques have their own complexities, are time-consuming, and require skilled technicians with extensive training to produce reliable results, and regardless of the method chosen, the recovery rate is generally low. The current standard protocol, method 1623 (released by the U.S. Environment Protection Authority),⁹ combines filtration and the immunomagnetic selection method, which gives only 53% recovery rate of *Giardia* (Table S1 in the [supplementary material](#)). Therefore, new purification methods are proposed to solve these issues.

In recent years, novel technologies have been developed to isolate *Giardia* from different sample types (Table S1 in the [supplementary material](#)). However, most of these techniques are merely an improvement to the currently existing methods, such as two-stage membrane-based filtration, and higher sensitivity

immunomagnetic methods.¹⁰ While these improved methods have increased the throughput and purity of the original methods, they still suffer from significantly lower and more variable recovery rates and require adept technicians to operate.^{6,11–13}

Microfluidic devices are widely used to separate and purify cells and particles from various samples due to their precise manipulation of individual microparticles inside the channels.^{14,15} These devices are classified as either active or passive. Active microfluidic devices use an external input to modulate particle behavior in the channel.^{16–18} These systems possess good sample recovery rates and yield high purity samples, yet the complicated operation, difficulty in fabrication, and low throughput characters restrain their application. Passive microfluidic devices rely on the hydrodynamic forces created by channel geometry and fluid flow to sort particles.¹⁹ Compared with active systems, passive microfluidic devices have a simpler design, are easier-to-operate, and are cheaper to produce. Some microfluidic devices have previously been demonstrated as capable of purifying *Giardia*,^{5,20–23} however, most of them have low throughput, complicated system settings, and are difficult to manufacture. More importantly, most of them are designed for purifying *Giardia* from relatively clean samples (such as drinking water), and their capability to process turbid samples, such as fecal samples in diagnostic settings, has not been demonstrated.

Polydimethylsiloxane (PDMS) is the most common material for making microfluidic devices. The advantages of PDMS microchannels are their low autofluorescence, optical transparency, and good biocompatibility. However, PDMS molds require hazardous materials and advanced equipment to fabricate. More importantly, the manufacturing of PDMS devices is a manual process, and due to the soft nature of PDMS, there is a significant risk of deformation and leakage under high flow rates and pressures. This has adverse effects on the functionality of the channel and causes chip instability problems in operation.^{24,25} It is, therefore, beneficial to develop a new method that addresses these common problems.

Taking the benefits of high-resolution and micrometer-scale additive manufacturing, 3D printing technologies have become popular in fabricating microfluidic devices. The devices produced by 3D printing are rigid in nature and are, therefore, less likely to deform or explode under pressure. Furthermore, cheap materials and a fast printing process make them favorable for use in the manufacture of prototype devices for commercialization.²⁶ Various methods exist for 3D printing a microchannel. 3D printers based on digital light processing (DLP) and stereolithography apparatus (SLA) proffer great promise and indeed have been widely adopted in the field where various microfluidic channels for different applications have been reported so far.^{27,28}

In our previous study, we proposed a simple, robust, and standardized 3D printing protocol for the fabrication of inertial microfluidic devices.²⁹ In this study, we employed this protocol to fabricate a trapezoidal spiral microfluidic device to separate *Giardia* from turbid samples with various sizes of contaminants, e.g., mouse fecal samples (Fig. 1). This device has a high resolution in particle separation, with a 75% *Giardia* recovery rate and 95% debris removal rate at 0.75 ml/min. Our characterization results reveal that the recovery rate is concentration dependent. The purity and number of *Giardia* recovered from turbid samples are clear enough to be directly observed under bright-field microscopy. Since improving the accuracy of giardiasis diagnosis will greatly benefit patients and overall public hygiene, this device can be used in parallel as a low-cost solution for large-scale purification of *Giardia* from fecal and environmental samples as well as food industry applications.

II. MATERIAL AND METHODS

A. Device fabrication

The device fabrication method was described in detail in our previous work [Fig. 2(a)].²⁹ In brief, it is comprised of a spiral microfluidic channel with trapezoidal cross section with heights of

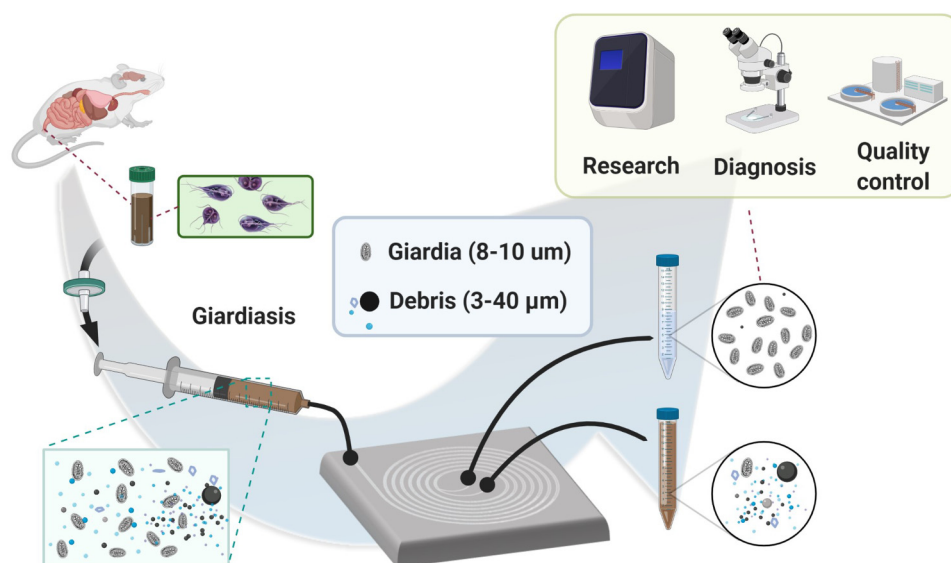


FIG. 1. The workflow, setup, and application of using inertial microfluidic device to separate *Giardia* from the fecal sample.

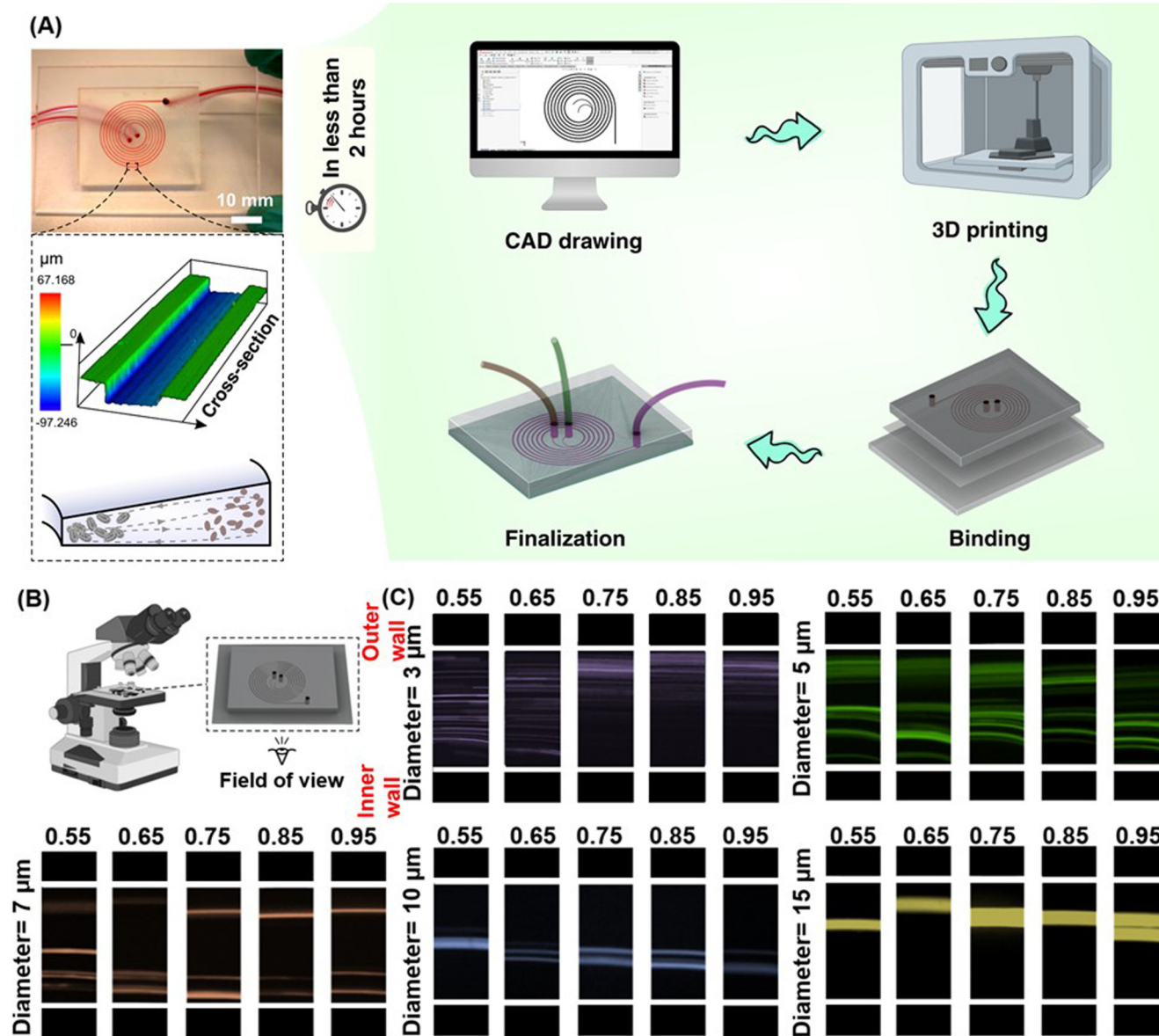


FIG. 2. (a) The manufacturing process of this device consists of four steps and takes less than 2 h. The device was designed by SolidWorks and then printed with a DLP 3D printer, washed by IPA, and cured again with UV light and finally bonded to PMMA sheet with double-coated adhesive tape. A bright-field picture of the device produced with our protocol and filled with red dye is to show the channel. The surface profilometry was performed with an unbonded channel (left). More details are given in Fig. S2 in the [supplementary material](#). The uniform color of each surface indicated that the surface of the chip was smooth and has relatively low surface roughness. (b) The experimental setup of this paper. The transparent PMMA base allowed easy observation of particle movement inside the channel. (c) The particle movement in the spiral device. Particles sized 3 μm were focused at the outer wall, 5 and 7 μm particles formed double band focusing, and 10 μm particles started focusing in the middle and shift to the inner wall from 0.65 ml/min. 15 μm particles were focused at the outer wall.

30 and 90 μm and a width of 300 μm . This was drafted using SolidWorks 2016, a commercially available CAD drawing software, and printed with a high resolution (30 μm XY) DLP 3D printer (MiiCraft Ultra 50, Hsinchu, Taiwan). The channel was designed as

an open channel with two sidewalls and a top wall. The bottom wall was open and faced toward the resin tank. Then, the part was sliced using the provided software with a slice thickness of 10 μm to make sure parts were of sufficient quality. After the device was

printed, it was washed with isopropyl alcohol (IPA) three times, dried by an air nozzle to remove any uncured resin on the surface, and was further cured by a 405 ± 5 nm UV light. Then, the device was bound to a PMMA substrate with double-coated adhesive tape (ARclear®, Adhesive Research) for the aim of the live monitoring of the channel.

B. Device characterization

Fluorescent microparticles with sizes of 3, 5, 7, 10, and 15 μm (Magsphere, USA) were used to assess the performance of the device. The beads were diluted in a 1:300 ratio in MACS buffer (Miltenyl Biotec, Australia), which contains bovine serum albumin (BSA) to prevent aggregation and sticking of beads to the channel tubing (Tygon tubing, inner diameter: 0.020 in., outer diameter: 0.060 in.). Then, the solution was added into a 10 ml syringe (BD plastic, BD Bioscience, USA), which was capped with a 1.5 mm precision tip (Adhesive dispensing Ltd.) and loaded onto the syringe pump (Fusion Touch, Chemyx Inc.). Screenshots of the particle's movement were taken and verified with the microscope image in CellSens (Olympus, USA).

C. Sample preparation and device setup

Two samples of heat-inactivated, raw *Giardia lamblia* cysts in mouse feces, as well as sucrose and percoll density gradient-centrifuged cyst samples (two samples each), were kindly supplied by Biopoint Ltd. (Sydney, Australia). Due to the wide variety of debris in the raw sample, a filtration step was necessary prior to processing the sample with the microfluidic device (debris can range up to millimeters size, causing blockages in the channel). The samples were subsequently filtered with a 40 μm pore size cell strainer (Corning, Australia) to remove large particles prior to running the experiment.

Different concentrations of samples were made by diluting the samples in different dilution factors (4, 6, and 10) and loaded into different 10 ml syringes (BD plastic, BD Bioscience, USA). The inner and outer outlet samples were collected separately in two 15 ml falcon tubes (Corning, Australia) for counting (Fig. S1 in the [supplementary material](#)). To further increase the purity, a sample from the target outlet was diluted to 10 ml with DPBS (Invitrogen, Australia) and loaded into the same syringe and proceeded through the device again. Then, all samples were collected to be counted in a flow cytometer. The results are displayed as concentration vs recovery and debris removal rate.

D. Sample imaging, counting, and data analysis

EasyStain antibody (Biopoint Pty Ltd) was used to stain the processed *Giardia*. For debris and *Giardia* counting, 100 μl of the samples from all outlets were mixed with 100 μl of EasyStain antibody, diluted in 800 μl DPBS in Trucount™ flow cytometry tubes (BD Bioscience, USA), and incubated at room temperature for 10 min. Then, samples were counted by a BD FACS Calibre flow cytometer (BD Bioscience, USA). Counts were performed in triplicate. For debris counting, the number of Trucount bead events was set to 500. The total numbers of *Giardia* and debris in each sample

were calculated by Eq. (1),

$$\text{Number of count} = \frac{49400}{500} \times \text{dilution factor (DF)} \times \text{volume (V)} \times \text{count}, \quad (1)$$

where 49 400 is the total number of beads in the batch of Trucount tubes used. The flow cytometer was set to stop when 500 Trucount bead events were recorded.

The percentage of *Giardia* recovered and debris eliminated were counted with Eqs. (2)–(4),³⁰

$$\text{Giardia}_{\text{Recovered}} = \frac{\text{Giardia}_{\text{inner}}}{\text{Giardia}_{\text{inner}} + \text{Giardia}_{\text{outer}}} \times 100\%, \quad (2)$$

$$\text{Debris} = \text{Total count} - \text{beads} - \text{Giardia}, \quad (3)$$

$$\text{Debris}_{\text{removed}} = \frac{\text{Debris}_{\text{outer}}}{\text{Debris}_{\text{inner}} + \text{Debris}_{\text{outer}}} \times 100\%. \quad (4)$$

We then used the forward scatter (FSC) and side scatter (SSC) parameters on the resulting cytometry plot to measure the overall purity. First, a large region was created, which included the range in which all *Giardia*-sized particles (including *Giardia* cysts themselves) would appear (200–10 000 on FSC and 300–10 000 on SSC). Within this region, a second smaller region was created to quantify intact, healthy *Giardia*. The location of this second region is based on the known size and granularity of healthy *Giardia*, which we have determined previously. The second smaller region falls between SSC 350–2200 and FSC 2000–5000.

A hemocytometer (Sigma-Aldrich, Australia) was used to visually observe the recovery and purity of the samples. A 10 μl sample from each tube was taken and loaded onto the hemocytometer; the microscopy process was performed using an IX70 microscope (Olympus, Japan), and snapshots were taken at 4 \times and 10 \times magnifications with bright-field view and green (FITC) fluorescent staining. Each observation was repeated three times.

III. RESULTS

A. Principles of inertial microfluidics

Cells and particles in a spiral microchannel experience inertial lift and Dean drag forces [Eqs. (5) and (6)]. The balance of these two forces moves the particles toward various equilibrium positions,³¹

$$F_L = \rho \left(\frac{U_{\text{max}}}{D_h} \right) C_L a^4, \quad (5)$$

$$F_D = 5.4 \times 10^{-4} \pi \mu D_e^{1.63} a. \quad (6)$$

In the inertial lift force (F_L) equation, ρ is the density, a is the particle diameter, D_h is the hydraulic diameter of the channel that can be calculated by $4A/P$ (A is the channel cross section and P is the channel perimeter), U_{max} is the maximum fluid velocity that can be approximated as $2 \times U_f$ where U_f is the average fluid velocity, and C_L is a dimensionless lift coefficient number whose sign and value depends on the channel Re ($Re = \rho U D_h / \mu$, U is the

average velocity and μ is the viscosity) and position of particles in the channel. When cells are migrating within a straight channel, they experience shear gradient and wall induced lift forces, both of which are constituents of inertial lift force. Shear gradient induced lift force pushes particles toward the channel walls. Once particles approach the vicinity of walls, a wall induced lift force pushes particles away from the wall. The balance of these two forces leads to the migration of particles into specific positions.

In spiral channels, however, particles experience another force in addition to inertial lift forces. This is the result of a velocity mismatch at the channel curvature, as specified by Eq. (6), which is the Dean drag force. De is the Dean number ($De = Re\sqrt{D_h/2R}$, R is the radius of curvature) used to characterize the strength of the Dean flow.^{32,33} Based on Eqs. (5) and (6), cells and particles with different diameters are potentially affected by different strengths of inertial lift ($F_L \propto a^4$) and Dean drag ($F_D \propto a$) forces. Thus, they occupy distinct lateral positions and can be isolated and collected through various outlets assigned at specific locations. Previous literature and research studies have demonstrated that particles are focused on the channel when the criteria of $Cr = a/D_h > 0.07$ is satisfied.³⁴ However, this number must be adjusted for hard chips (3D-printed microchannels). Due to the inflation of PDMS-made microchannels under high pressure, focusing positions of particles would be different from theoretical calculation, while the hard chip we presented here does not have this problem. According to flow cytometry and microscopy results, the *Giardia* in this experiment were $\sim 8\text{--}10\text{ }\mu\text{m}$ in diameter, and most of the debris were around $3\text{ }\mu\text{m}$. By carefully analyzing the size of *Giardia* and commonly associated debris in this study, we have shown that a 3D-printed, rigid, spiral channel with a trapezoidal cross section and a width of $300\text{ }\mu\text{m}$, heights of 30 and $90\text{ }\mu\text{m}$, initial diameter of $8\text{ }\mu\text{m}$, and pitch of $1\text{ }\mu\text{m}$ with seven loops is able to separate *Giardia* from debris. With this device, *Giardia* could be focused at the inner wall while the majority of debris could be focused at the outer wall and collected from their specific outlets.

B. Device characterization

The device was then characterized by recording videos of fluorescent microparticles passing through the channel [Fig. 2(b)]. Spiral microfluidic devices have long been used for separating particles of different sizes,^{35,36} and the dimension of the microfluidic channel has a direct impact on device performance. The pressure drop of our designed channel is around 80 KPa , and the maximum velocity at flow rate of 0.75 ml/min is 1.4 m/s . Our previous publication showed that this pressure does not compromise the viability of cancer cell lines,²⁵ and, therefore, it is unlikely to compromise the viability of *Giardia*. Figure 2(c) also shows the velocity distribution of a cross section near the channel outlets, which reveals that the distribution of velocity is not symmetrical due to the trapezoidal shape of the channel cross section, as the main reason for particle/cell separation in spiral microchannels. Next, we introduced fluorescent microparticles into our device to mimic the movement of *Giardia* and different sizes of contaminants. The results [Fig. 2(c)] show that $3\text{ }\mu\text{m}$ particles are dispersed at a low flow rate and then get focused at the outer wall; the focusing band was tight when the flow rate is above 0.75 ml/min . $5\text{ }\mu\text{m}$ particles formed a loose double

band focusing while $7\text{ }\mu\text{m}$ beads formed a tight double band focusing across all flow rates. $10\text{ }\mu\text{m}$ particles formed a tight band close to the inner wall when the flow rate is higher than 0.65 ml/min , and $15\text{ }\mu\text{m}$ particles were focused in the outer outlet, but gradually shifting toward the inner outlet as the flow rate increased, which we assume will be focused in the inner outlet when the flow rate is higher than 1.00 ml/min . In the real scenario, the debris and contaminants in the samples have irregular shapes and sizes. The orientation of the debris continually changed the balance of the inertial forces that they experienced. Hence, we designed the ratio of the inner outlet area to the outer outlet area to be 0.29 . The larger inner outlet area can guide most of the irregularly shaped debris toward the outer outlet, simply as the area of the outer outlet is larger than the inner outlet. In this way, smaller sized debris also have a higher chance of going to the outer outlet.

C. Purification of *Giardia* from commercial samples

Figure 3(a) shows the extremely high concentration of debris in the sample, and Fig. 3(b) shows the size of most of the debris in the commercial samples which are $>3\text{ }\mu\text{m}$. Therefore, to obtain the best purification efficiency, 0.75 ml/min flow rate was used in all following experiments. The particle concentration of samples is an important factor that affects the recovery rate, as the particle-particle interaction in an over-concentrated sample disturbs particle behavior in the channel³⁷ and disrupts the focusing position of microparticles inside the channel. Our results in Fig. 3(c) were consistent with this hypothesis: higher particle concentration resulted in lower *Giardia* recovery rate. In contrast, low particle concentration gave higher *Giardia* recovery rates. At the same time, the debris clearance was shown to remain consistently above 85% regardless of the particle concentration. (Table S2 in the supplementary material). The best result of one-round separation groups showed that the *Giardia* recovery rate reached $75 \pm 0.7\%$ when the debris removal rate was $95 \pm 2.4\%$, indicating the device has a strong capability for removing multiple sizes of contaminants. This was also verified by flow cytometry [Fig. 3(d)]. Although $>70\%$ of *Giardia* was lost in the highest particle concentration groups, the debris removal rate remained $>85\%$. Moreover, the purified *Giardia* were clean enough to be observed under typical bright-field microscopy without staining [Fig. 3(e)], in contrast to the non-purified sample [Figs. 3(a) and 3(b)] in which *Giardia* were much more difficult to discern due to the high degree of particulate contamination.

To demonstrate the effectiveness of using this device for extracting *Giardia* from drinking water samples, a sample was twice purified through the device [Fig. 4(a)]. This sample was first diluted 10 times and passed through the device, and then the inner outlet sample was collected and processed through the device a second time using the same settings [Fig. 4(b)]. In this test, the recovery rate of *Giardia* approached $88 \pm 1.1\%$, with a debris-cleaning rate of $72 \pm 5.4\%$ [the lowest concentration group of Fig. 3(c)]. This decline in the cleaning rate is likely due to the low initial quantity of debris in this sample and/or the relatively higher number of $10\text{ }\mu\text{m}$ debris compared to the impurified samples. The total *Giardia* recovery rate from two rounds of purification was 65.38% , and the total debris removal rate was 98.6% .

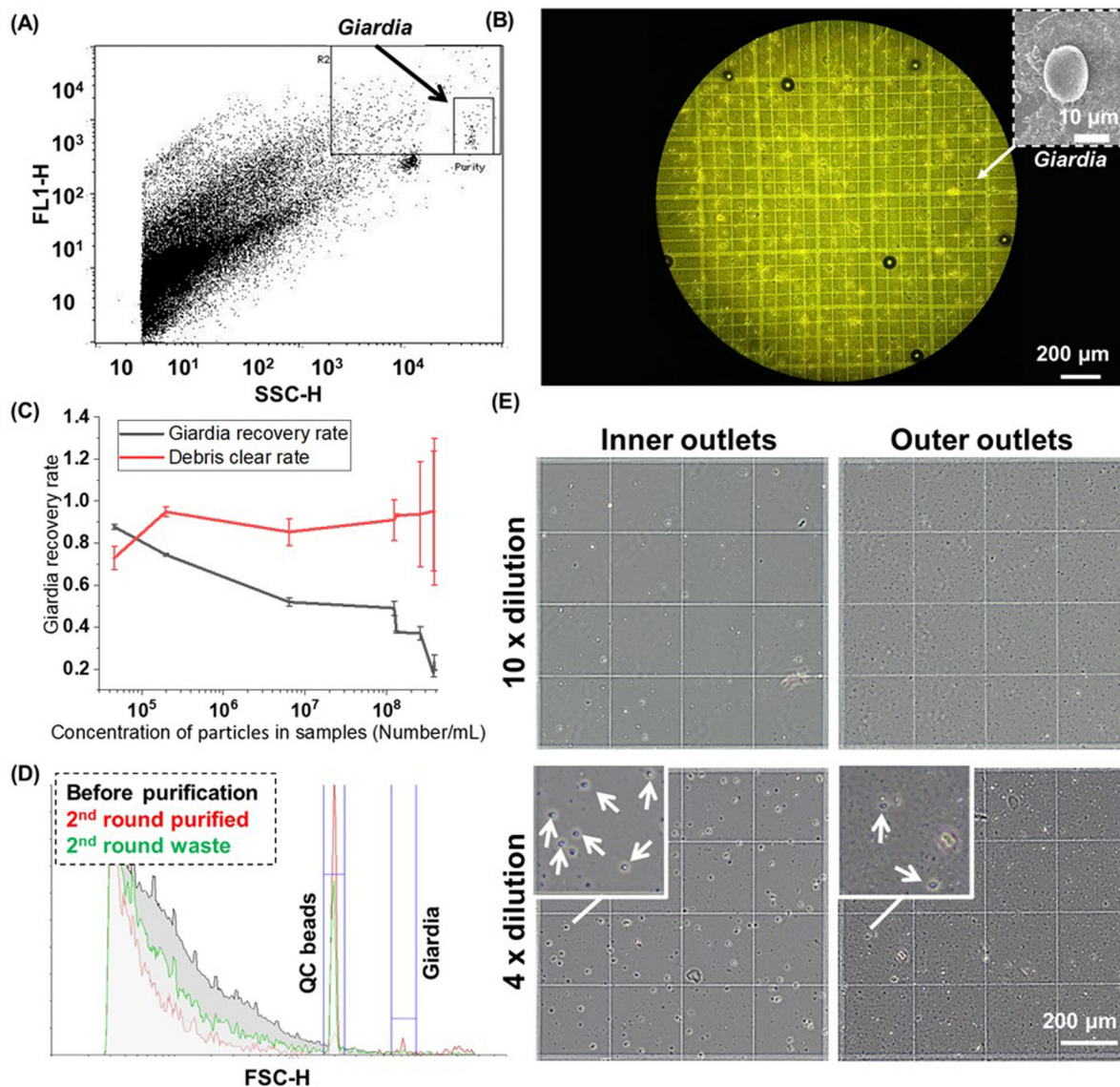


FIG. 3. (a) and (b) showed the turbidity of the undiluted sample with flow cytometry and optical image and showed most of the debris are much smaller than the *Giardia*. The top right corner of (b) showed the SEM image of the sample before separation, and the rare *Giardia* sample was surrounded by concentrated debris. (c) The relationship between particle concentrations in the sample and *Giardia* recovery rate. The higher the concentrations, the lower the *Giardia* recovery rate, while the debris removal rate is constantly high across high concentration. The *Giardia* recovery rate of one round of purification was 75%, and the debris removal rate was higher than 95%. The lowest concentration group was one sample that had been purified twice. The results showed that while the debris removal rate dropped to 72%, the recovery rate increased further to 87% due to less particle interference in the device. (d) The flow cytometry results of the sample indicated that most of the debris are much smaller than *Giardia*, and the concentration is extremely high. After purification, the *Giardia* peak becomes obvious while the concentration of debris decreases hugely. (e) The outlet samples of two different concentrations. Both outer outlet results showed great number of debris, and the two inlets showed a good amount of *Giardia*.

D. Purification of *Giardia* from raw fecal samples

We then tested the capability of the device to purify *Giardia* from raw mouse fecal samples. Two fecal samples were diluted before being proceeded through the device. Compared to the commercial samples, raw samples had lower *Giardia* concentration and contained

more debris of similar size to the *Giardia* cysts. The separation results showed that the inner outlet contains debris and *Giardia* with a size of 10 µm, while the outer outlet contained a much greater variety of debris—further demonstrating the capability of the device to remove the debris larger than 15 µm at 0.75 ml/min flow rate [Fig. 5(b) and

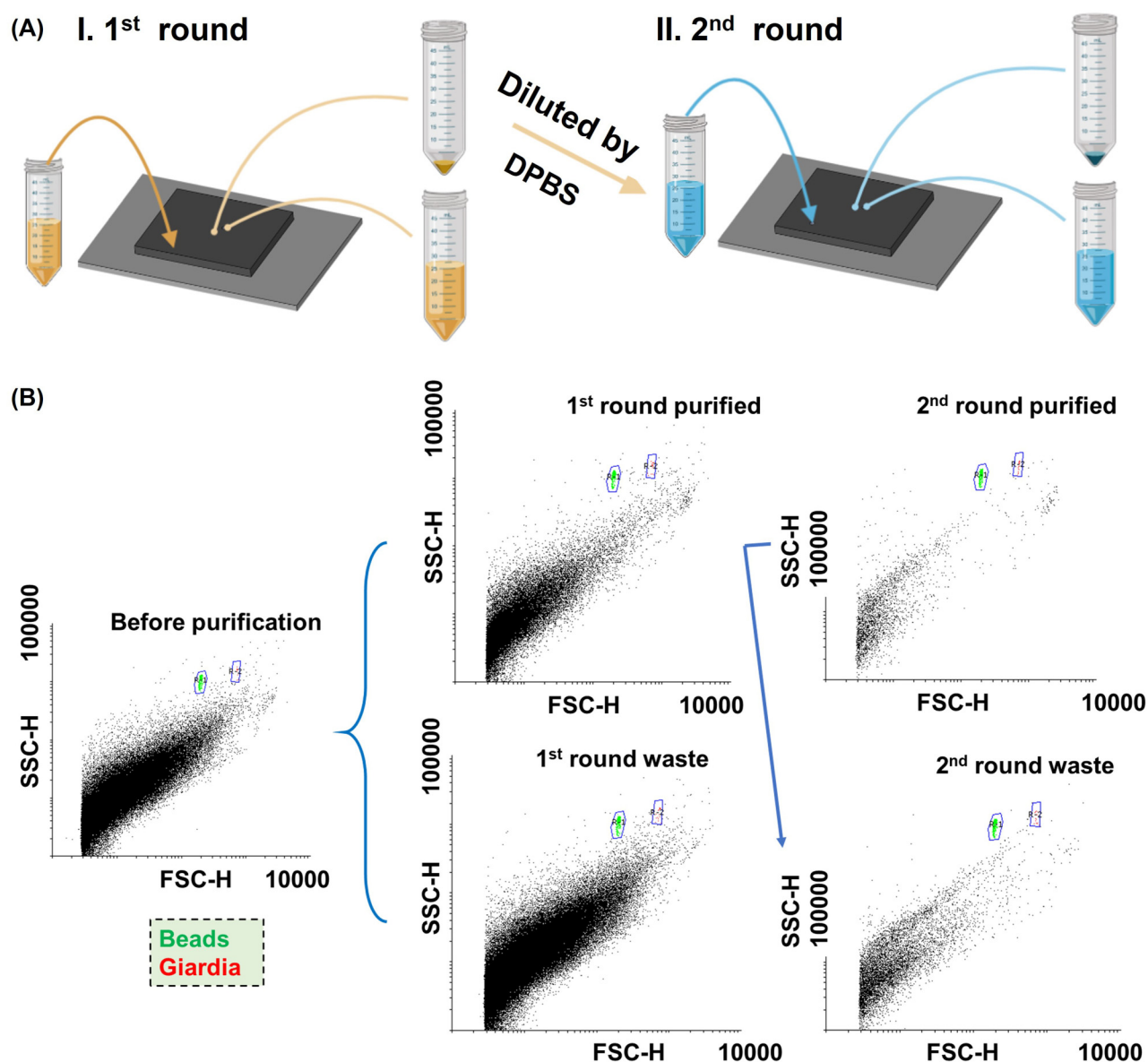


FIG. 4. (a) The process of two-round purification. The inner outlet sample of the first-round purification was diluted by DPBS to 8 ml again and proceeded through the spiral device. (b) The flow cytometry results of two-round purification. After two rounds of purification, the population of *Giardia* was clearly visible in the graph.

Video S1 in the [supplementary material](#). The separation results outlined in [Fig. 5\(c\)](#) show a >70% debris removal rate ($73.68 \pm 33.18\%$ at least) in all samples with more than 20% *Giardia* recovery rate ($20.12 \pm 1.0\%$ at least). [Figure 5\(d\)](#) shows that after the extraction process, the concentration of *Giardia* in the sample was not diluted compared to the raw fecal samples and it could be two times more concentrated, while the volume was only 1/3 of the input. This is of great help for diagnosis since *Giardia* concentration remains the same while more than 70% of the debris removed from the sample.

In each purified sample, the *Giardia* cysts could be distinguished under bright-field microscopy without staining [[Fig. 5\(e\)](#)].

IV. DISCUSSION

A. Optimizing the 3D-printed inertial microfluidic channel

The application of 3D printing technology in microfabrication is a nascent field compared to PDMS-based soft lithography, which

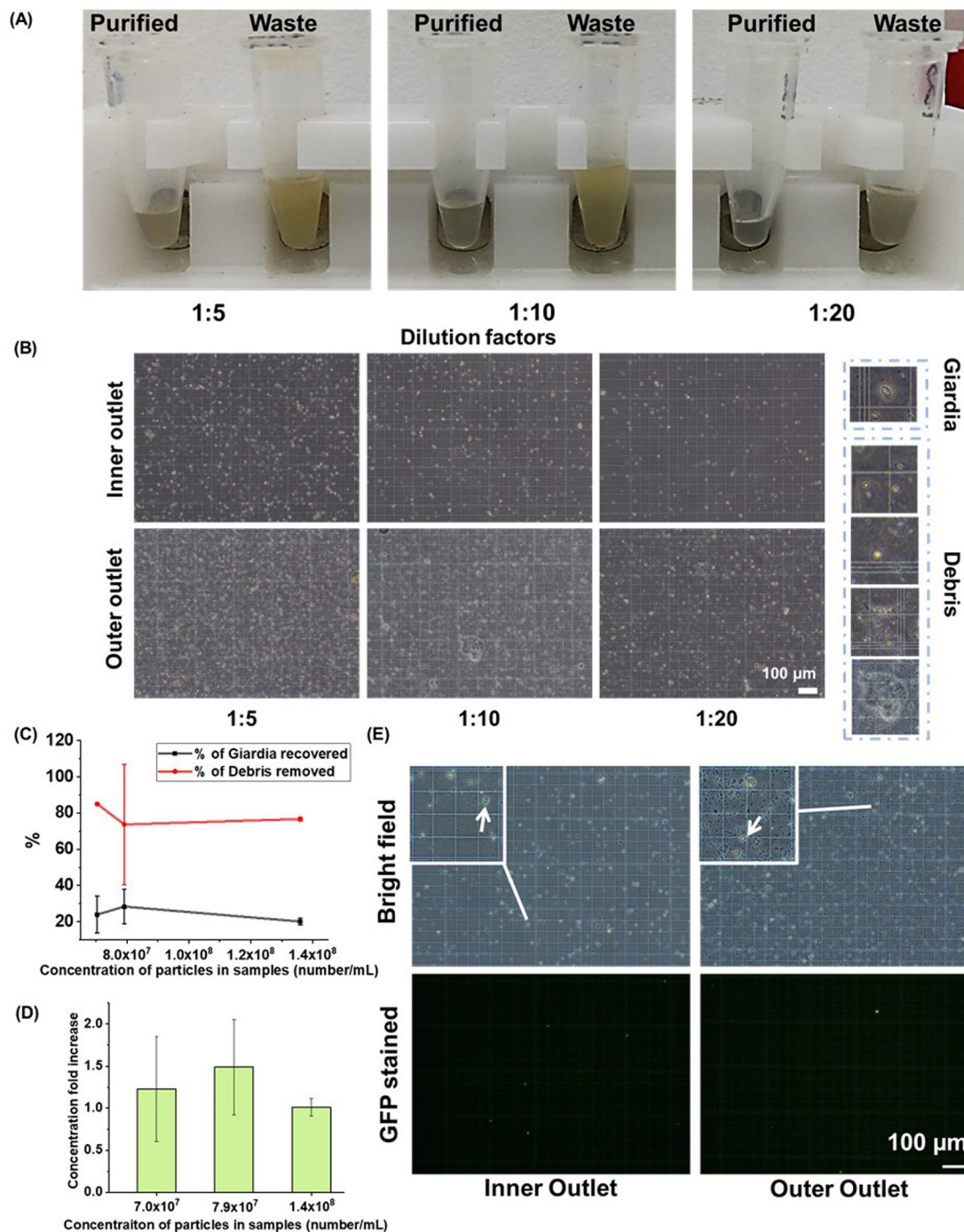


FIG. 5. (a) Optical image of the purified *Giardia* fecal samples compares to the waste of the purification. Different dilutions of raw samples were used to compare the outcome. (b) The separation results of the raw samples with different dilution factors under a 10 \times microscope. The outer outlet results showed that the device can dispose debris with sizes smaller than 10 and larger than 15 μm . (c) The *Giardia* recovery rate and debris removing rate of raw samples proceeded through the spiral device. The samples from left to right correspond to 1:5, 1:10, and 1:20 dilutions. (d) The *Giardia* concentration fold increase (concentration after purification/concentration before purification) of the purified samples compared to the raw samples. (e) The outlets samples of the 1:5 diluted *Giardia* sample. There were more similar size debris compared to the purified commercial samples, but the *Giardia* were still easily purified without staining.

has been the frontrunner in the fabrication of microfluidic devices for more than two decades.³⁸ However, PDMS-based devices are vulnerable to structural problems such as inflated channels and a high risk of delamination under high pressure. In inertial microfluidic devices, the change of channel dimensions affects the focusing results of cells and particles, and this is one of the causes of inaccurate Computational Fluid Dynamics modeling of particle motion.³⁹ These problems limit the development and investigation of particle behavior in passive microfluidics. 3D-printed technologies bring new tools for solving these problems by their ability to fabricate physically stable devices and pattern complex and customizable geometries within a short time. The printing protocols and device settings provided by the printer manufacturers are based on the theoretical capabilities of the hardware; thus, the optimization of printing parameters is required to produce good quality devices.⁴⁰ Currently, whole-channel printing has been limited by printer resolution, accuracy, and the need for debris removal from the channel networks. DLP printers use the high sensitivity feature of the digital light engine to achieve high-resolution printing.⁴¹ However, commercially available DLP printers cannot print a transparent, small, implanted channel (known as a closed chip) as the resin residue in the channel is extremely hard to remove and has a high chance of curing in the channel during the printing process.

In this paper, we designed and fabricated a trapezoidal cross-sectional spiral microchannel with an area of $18000\ \mu\text{m}^2$, $300\ \mu\text{m}$ width, $30\ \mu\text{m}$ lower wall, and $90\ \mu\text{m}$ higher wall. With our revised protocol, the machine can print a channel with precise geometry and smooth topography, proven by surface profilometry [Fig. 2(a)]. These precise dimensions are essential for our application since changing the height of the chip might fail to separate $3\ \mu\text{m}$ and $10\ \mu\text{m}$ particles. Smaller channel dimensions can focus particles sufficiently and can be produced with our protocol, though achieving relatively high flow rates is difficult in these channels. In contrast, larger channels fail to focus $3\ \mu\text{m}$ particles in the outer outlet and, therefore, are less effective in removing debris (Fig. S3 in the [supplementary material](#)). Based on these trade-offs, the proposed microchannel outlined in this paper is the best candidate for *Giardia* separation from dirty samples. The high *Giardia* recovery rate in this two-round purification group indicates that the device is also capable of recovering *Giardia* from the water sample (Fig. 4).

B. Significance of this device and future applications

Purifying *Giardia* from turbid samples is challenging due to the high concentrations of debris with widely ranging sizes and shapes often present in the samples. In a pre-centrifuged sample (commercial sample), the ratio of *Giardia* to debris can be as low as 1:1000—which makes identifying small quantities of *Giardia* in such samples extremely difficult. This degree of contamination creates further difficulties in microscopic analysis of the *Giardia* cysts, as well as for biochemical, molecular, and proteomic analysis.

Microscopic diagnosis is labor-intensive, inaccurate, prone to human error,⁶ and requires multiple stool samples from different days to make an accurate diagnosis.^{8,42} Although newly developed methods, including molecular and antibody-based techniques, offer more accurate platforms for giardiasis diagnosis, microscopy is still

considered the gold standard for diagnosis⁴³ since it is straightforward, cheap, and it clarifies the infection stage of the patients while identifying the presence of other pathogens simultaneously.⁴⁴ These factors make microscopic analysis essential, particularly in developing countries where access to more advanced diagnostic tools is limited.

The need for high purity samples in *Giardia* research is even greater than in clinical diagnosis. Contaminants in feces can inhibit PCR reactions, increase the chance of non-specific antibody binding, and increase the volume of reagents used.^{6,8,42} Current purification techniques such as centrifugation-based methods cannot yield a clean enough population to perform these analyses. For example, the *Giardia* sample used in this experiment was purified from mouse feces by percoll density gradient centrifugation, yet the total number of particles in the resulting “purified” sample was still extremely high ($\sim 1 \times 10^9$ particles/ml). In addition to the low purity and recovery rate, the throughput of centrifugation-based methods is limited by the capacity of the centrifuge.⁶ Larger centrifuges can handle larger sample volumes at a time; however, this rapidly becomes a costly endeavor as the price of these devices is proportional to the volume of the sample it can handle. Moreover, centrifugation-based methods involve extensive manual handling and are susceptible to losses during the dewatering steps. Manual handling further increases the cost of purification and potentially exposing the technician to the risk of infection, while losses of *Giardia* reduce the output and increase the cost. Immunomagnetic-based methods are preferred as the final step of purification due to the high specificity of the method.⁶ Immunomagnetic separation methods generally have a low efficiency and recovery rate when applied to either raw samples or samples with a large volume. In large sample volumes, this is due to magnetic beads having a lower chance of contacting the target particles, meaning that a very large amount of beads would be required to effectively capture target cysts (this results in a high cost, and the price of immunomagnetic bead kits is expensive, which is the major drawback for the industrial aspect). In raw samples, excessive debris can also lead to non-specific binding on the beads. Purifying *Giardia* from commercial samples is important for industrial applications. Commercially available *Giardia* stock preparations have an extremely high cyst concentration and are relatively free of particles of similar size to *Giardia*. However, Fig. S4 in the [supplementary material](#) shows that the commercially available *Giardia* samples can still be highly turbid, and the quality of each batch varies. Further purification steps, including MACS and FACS are always necessary before applying them for research, and these two methods require antibody labeling of the samples. Here, we have developed an inertial microfluidic device that can both aid the sample preparation process for microscopic analysis and substitute further purification processes required for *Giardia* purification in the industry. Inertial microfluidic technology has high throughput, is simple to manufacture and operate, and has a low cost and a high recovery rate. For example, a 10 ml sample takes 13 min to process and much larger throughputs can be achieved by paralleling the channels.⁴⁵ The device took 1 h to be automatically produced by the printer; only one pump is required to operate, and the device operating flow rate is adaptable ($>0.65\ \text{ml/min}$). This lowers the level of expertise required for diagnosis while

maintaining the low cost and rapid characteristics of microscopic analysis. The device costs less than 1\$ AUD to produce, and it is disposable, eliminating the risk of cross-contamination. Finally, compared to other microfluidic devices, this device has shown the ability to proceed extremely turbid samples with various debris sizes and types, which has not been demonstrated by any other device or approach so far. The *Giardia* in the sample is easily distinguishable even under low magnification bright-field microscopy after processing [Fig. 3(d)]. The recovery rate and debris clearing rate of raw samples are lower than in pre-concentrated samples, and flow cytometer counts showed great variability. There are two possible reasons for this observed variability: (1) The raw samples contain a greater variety of debris, including protein aggregates, which may change the viscosity of the sample⁴⁶ and, therefore, disturb the focusing efficiency of the device; or (2) the raw samples contain greater number of large debris ($>10\mu\text{m}$), which might interfere with *Giardia* during focusing. Nonetheless, although the recovery rate was low, the concentration of *Giardia* in the inner outlet sample was as high as the raw samples and increases with dilution factor [Fig. 5(d)]. This is greatly helpful in the diagnostic process since *Giardia* concentration is maintained in the sample while massively reducing the debris content.

The high *Giardia* recovery rate in the two-round purification group [Fig. 3(e)] potentially indicates that the device is also capable of recovering *Giardia* from drinking water samples and has a robust ability to eliminate debris. Moreover, this device can be used to purify other pathogens or intestinal bacteria in fecal samples. Figure 2(c) shows that this device can focus microparticles with diameter of $10\mu\text{m}$ when the flow rate is higher than 0.65 ml/min . When the flow rate increased to 0.95 ml/min , $15\mu\text{m}$ particles shifted toward the inner wall as well. This shows the potential of the device to purify other microbes commonly found in the digestive system with a size $>10\mu\text{m}$, such as *Diphyllobothrium latum*, intestinal *Entamoeba*, or *Chilomastix mesnili*. This is important considering the emerging research interest in intestinal microbial infections and their impacts on not only our digestive systems but also on neural systems.^{47,48} With the 3D-printed chip, this device has the potential to integrate into multiple downstream settings, such as increasing the recovery rate by reprocessing the waste outlet sample through the device, or scale-up by paralleling and stacking multiple devices together, like other inertial microfluidic devices previously shown.^{15,45}

V. CONCLUSION

In this paper, we have demonstrated a low-cost, rapidly manufacturable spiral microfluidic device to purify *Giardia* from significantly turbid mouse fecal samples. Due to the manufacturing protocol we applied here, a spiral microchannel with a trapezoidal cross section, width of $300\mu\text{m}$, and heights of 30 and $90\mu\text{m}$ ensures the *Giardia* focus at the inner outlet while debris with sizes <5 and $>15\mu\text{m}$ focus on the outer wall. The *Giardia* recovery rate depends on the concentration of the sample. It reached as high as 87.76% in a clean sample, which is sufficient for use in the detection of pathogens in water sources, while maintaining a high recovery rate of 75% in one round of purification of pre-centrifuged fecal samples. In addition to the high recovery rate, the debris-cleaning rate is maintained

at $>85\%$ in just one round of purification even when the input particle concentration is as high as 3×10^8 particles/ml. In raw fecal samples, although the recovery rate was low, more than 70% of debris removal rate was achieved, and after the purification, *Giardia* can be clearly observed with a $4\times$ microscope nosepiece, which greatly benefits the diagnosis accuracy of giardiasis. To the best of our knowledge, this is the first time a microfluidic device has been used to proceed extremely turbid samples for the purpose of purifying a target pathogen. The turbid samples contained contaminants of various types and morphologies, and our device was able to purify *Giardia* from such contaminants without the addition of any chemical sedimentation agents or using any complex apparatus. The device was operated with only one syringe pump, which hugely simplifies the equipment and expertise needed. We also believe that this device has the potential to be scaled-up for industrial applications by paralleling and multiplying the chip, as has been demonstrated with other inertial microfluidic devices.

SUPPLEMENTARY MATERIAL

See the [supplementary material](#) for the comparison and summary for recent technologies used in *Giardia* isolation, more device characterization, sample turbidity, and a video of device operation with the raw sample.

ACKNOWLEDGMENTS

M.E.W. would like to acknowledge the support from the Australian Research Council through Discovery Project Grants (Nos. DP170103704 and DP180103003) and the National Health and Medical Research Council through the Career Development Fellowship (No. APP1143377). The schematic in Fig. 1 was made with Biorender.com.

AUTHOR DECLARATIONS

Conflict of Interest

The authors have no conflicts to disclose.

DATA AVAILABILITY

The data that support the findings of this study are available within the article and its [supplementary material](#).

REFERENCES

- ¹M. E. Alvarado and M. Wasserman, "Quick and efficient purification of *Giardia intestinalis* cysts from fecal samples," *Parasitol. Res.* **99**(3), 300–302 (2006).
- ²WHO, "Microbial aspect," in *Guidelines for Drinking-Water Quality*, 4th ed. (World Health Organization, 2011), Chap. 7.
- ³R. D. Adam, "Biology of *Giardia lamblia*," *Clin. Microbiol. Rev.* **14**(3), 447–475 (2001).
- ⁴G. S. Logsdon, J. M. Symons, R. L. Hoye, Jr., and M. M. Arozarena, "Alternative filtration methods for removal of *Giardia* cysts and cyst models," *J. Am. Water Works Assoc.* **73**(2), 111–118 (1981).
- ⁵K. R. Ganz, L. Clime, J. M. Farber, N. Corneau, T. Veres, and B. R. Dixon, "Enhancing the detection of *Giardia duodenalis* cysts in foods by inertial microfluidic separation," *Appl. Environ. Microbiol.* **81**(12), 3925–3933 (2015).
- ⁶D. S. Zarlenga and J. M. Trout, "Concentrating, purifying and detecting water-borne parasites," *Vet. Parasitol.* **126**(1–2), 195–217 (2004).

- ⁷M. W. Dryden, P. A. Payne, and V. Smith, "Accurate diagnosis of *Giardia* spp and proper fecal examination procedures," *Vet. Ther.* **7**(1), 4–14 (2006).
- ⁸H. Hooshyar, P. Rostamkhani, M. Arbabi, and M. Delavari, "*Giardia lamblia* infection: Review of current diagnostic strategies," *Gastroenterol. Hepatol. Bed Bench.* **12**(1), 3 (2019).
- ⁹C. L. DiGiorgio, D. A. Gonzalez, and C. C. Huitt, "*Cryptosporidium* and *Giardia* recoveries in natural waters by using Environmental Protection Agency method 1623," *Appl. Environ. Microbiol.* **68**(12), 5952–5955 (2002).
- ¹⁰K. Shepherd and A. Wyn-Jones, "An evaluation of methods for the simultaneous detection of *Cryptosporidium* oocysts and *Giardia* cysts from water," *Appl. Environ. Microbiol.* **62**(4), 1317–1322 (1996).
- ¹¹Q. Ramadan, L. Christophe, W. Teo, S. Li, and H. H. Feng, "Flow-through immunomagnetic separation system for waterborne pathogen isolation and detection: Application to *Giardia* and *Cryptosporidium* cell isolation," *Anal. Chim. Acta* **673**(1), 101–108 (2010).
- ¹²M. E. Warkiani, L. Chen, C.-P. Lou, H.-B. Liu, R. Zhang, and H.-Q. Gong, "Capturing and recovering of *Cryptosporidium parvum* oocysts with polymeric micro-fabricated filter," *J. Membr. Sci.* **369**(1), 560–568 (2011).
- ¹³L. Chen, M. E. Warkiani, H.-B. Liu, and H.-Q. Gong, "Polymeric micro-filter manufactured by a dissolving mold technique," *J. Micromech. Microeng.* **20**(7), 075005 (2010).
- ¹⁴C. A. Aya-Bonilla, G. Marsavela, J. B. Freeman, C. Lomma, M. H. Frank, M. A. Khattak *et al.*, "Isolation and detection of circulating tumour cells from metastatic melanoma patients using a slanted spiral microfluidic device," *Oncotarget* **8**(40), 67355–67368 (2017).
- ¹⁵T. Kwon, H. Prentice, J. Oliveira, N. Madziva, M. E. Warkiani, J. P. Hamel *et al.*, "Microfluidic cell retention device for perfusion of mammalian suspension culture," *Sci. Rep.* **7**(1), 6703 (2017).
- ¹⁶J. Zhang, S. Yan, D. Yuan, G. Alici, N.-T. Nguyen, M. Ebrahimi Warkiani, and W. Li, "Fundamentals and applications of inertial microfluidics: A review," *Lab Chip* **16**(1), 10–34 (2016).
- ¹⁷S. R. Bazaz, A. A. Mehrizi, S. Ghorbani, S. Vasilescu, M. Asadnia, and M. E. Warkiani, "A hybrid micromixer with planar mixing units," *RSC Adv.* **8**(58), 33103–33120 (2018).
- ¹⁸D. Morshedi Rad, M. Alsatat Rad, R. Razavi Bazaz, N. Kashaninejad, D. Jin, and M. Ebrahimi Warkiani, "A comprehensive review on intracellular delivery," *Adv. Mater.* **33**(13), 2005363 (2021).
- ¹⁹P. Sajeesh and A. K. Sen, "Particle separation and sorting in microfluidic devices: A review," *Microfluid. Nanofluid.* **17**(1), 1–52 (2014).
- ²⁰Y. Liu, D. Hartono, and K.-M. Lim, "Cell separation and transportation between two miscible fluid streams using ultrasound," *Biomicrofluidics* **6**(1), 012802 (2012).
- ²¹R. Lejard-Malki, J. Follet, A. Vlandas, and V. Senez, "Selective electrohydrodynamic concentration of waterborne parasites on a chip," *Lab Chip* **18**(21), 3310–3322 (2018).
- ²²M. Jimenez and H. Bridle, "Microfluidics for effective concentration and sorting of waterborne protozoan pathogens," *J. Microbiol. Methods* **126**, 8–11 (2016).
- ²³N. M. Pires, "Recovery of *Cryptosporidium* and *Giardia* organisms from surface water by counter-flow refining microfiltration," *Environ. Technol.* **34**(17–20), 2541–2551 (2013).
- ²⁴N. Bhattacharjee, A. Urrios, S. Kang, and A. Folch, "The upcoming 3D-printing revolution in microfluidics," *Lab Chip* **16**(10), 1720–1742 (2016).
- ²⁵S. Razavi Bazaz, H. A. Amiri, S. Vasilescu, A. Abouei Mehrizi, D. Jin, M. Miansari, and M. Ebrahimi Warkiani, "Obstacle-free planar hybrid micro-mixer with low pressure drop," *Microfluid. Nanofluid.* **24**(8), 61 (2020).
- ²⁶J. Shrestha, S. T. Ryan, O. Mills, S. Zhand, S. Razavi Bazaz, P. M. Hansbro *et al.*, "A 3D-printed microfluidic platform for simulating the effects of CPAP on the nasal epithelium," *Biofabrication* **13**(3), 035028 (2021).
- ²⁷J. Shrestha, M. Ghadiri, M. Shanmugavel, S. Razavi Bazaz, S. Vasilescu, L. Ding, and M. Ebrahimi Warkiani, "A rapidly prototyped lung-on-a-chip model using 3D-printed molds," *Organs Chip* **1**, 100001 (2019).
- ²⁸M. Chai, S. Razavi Bazaz, R. Daiyan, A. Razmjou, M. Ebrahimi Warkiani, R. Amal, and V. Chen, "Biocatalytic micromixer coated with enzyme-MOF thin film for CO₂ conversion to formic acid," *Chem. Eng. J.* **426**, 130856 (2021).
- ²⁹S. Razavi Bazaz, O. Rouhi, M. A. Raoufi, F. Ejeian, M. Asadnia, D. Jin, and M. Ebrahimi Warkiani, "3D printing of inertial microfluidic devices," *Sci. Rep.* **10**(1), 5929 (2020).
- ³⁰G. Segre and A. Silberberg, "Radial particle displacements in Poiseuille flow of suspensions," *Nature* **189**(4760), 209 (1961).
- ³¹A. Agarwal, A. Mulgund, A. Hamada, and M. R. Chyatte, "A unique view on male infertility around the globe," *Reprod. Biol. Endocrinol.* **13**, 37 (2015).
- ³²M. R. Condina, B. A. Dilmetz, S. Razavi Bazaz, J. Meneses, M. Ebrahimi Warkiani, and P. Hoffmann, "Rapid separation and identification of beer spoilage bacteria by inertial microfluidics and MALDI-TOF mass spectrometry," *Lab Chip* **19**(11), 1961–1970 (2019).
- ³³A. Mashhadian and A. Shamloo, "Inertial microfluidics: A method for fast prediction of focusing pattern of particles in the cross section of the channel," *Anal. Chim. Acta* **1083**, 137–149 (2019).
- ³⁴D. Di Carlo, D. Irimia, R. G. Tompkins, and M. Toner, "Continuous inertial focusing, ordering, and separation of particles in microchannels," *Proc. Natl. Acad. Sci. U.S.A.* **104**(48), 18892–18897 (2007).
- ³⁵M. E. Warkiani, B. L. Khoo, L. Wu, A. K. Tay, A. A. Bhagat, J. Han, and C. T. Lim, "Ultra-fast, label-free isolation of circulating tumor cells from blood using spiral microfluidics," *Nat. Protoc.* **11**(1), 134–148 (2016).
- ³⁶A. S. Rzhetskiy, S. Razavi Bazaz, L. Ding, A. Kapitannikova, N. Sayyadi, D. Campbell *et al.*, "Rapid and label-free isolation of tumour cells from the urine of patients with localised prostate cancer using inertial microfluidics," *Cancers* **12**(1), 81 (2020).
- ³⁷D. Di Carlo, "Inertial microfluidics," *Lab Chip* **9**(21), 3038–3046 (2009).
- ³⁸M. A. Raoufi, S. Razavi Bazaz, H. Niazmand, O. Rouhi, M. Asadnia, A. Razmjou, and M. Ebrahimi Warkiani, "Fabrication of unconventional inertial microfluidic channels using wax 3D printing," *Soft Matter* **16**(10), 2448–2459 (2020).
- ³⁹R. Bazaz S, A. Mashhadian, A. Ehsani, S. Saha, T. Krueger, and M. Ebrahimi Warkiani, "Computational inertial microfluidics: A review," *Lab Chip* **20**(6), 1023–1048 (2020).
- ⁴⁰S. Razavi Bazaz, N. Kashaninejad, S. Azadi, K. Patel, M. Asadnia, D. Jin, and M. Ebrahimi Warkiani, "Rapid soft lithography using 3D-printed molds," *Adv. Mater. Technol.* **4**(10), 1900425 (2019).
- ⁴¹J. Y. Han, B. Krasniqi, J. Kim, M. Keckley, and D. L. DeVoe, "Miniaturization of hydrocyclones by high-resolution 3D printing for rapid microparticle separation," *Adv. Mater. Technol.* **5**, 1901105 (2020).
- ⁴²S. P. Johnston, M. M. Ballard, M. J. Beach, L. Causer, and P. P. Wilkins, "Evaluation of three commercial assays for detection of *Giardia* and *Cryptosporidium* organisms in fecal specimens," *J. Clin. Microbiol.* **41**(2), 623–626 (2003).
- ⁴³R. Soares and T. Tasca, "Giardiasis: An update review on sensitivity and specificity of methods for laboratorial diagnosis," *J. Microbiol. Methods* **129**, 98–102 (2016).
- ⁴⁴H. A. El-Nahas, D. A. Salem, A. A. El-Henawy, H. I. El-Nimr, H. A. Abdel-Ghaffar, and A. M. El-Meadawy, "*Giardia* diagnostic methods in human fecal samples: A comparative study," *Cytom. B Clin. Cytom.* **84B**(1), 44–49 (2013).
- ⁴⁵L. Wang and D. S. Dandy, "A microfluidic concentrator for cyanobacteria harvesting," *Algal. Res.* **26**, 481–489 (2017).
- ⁴⁶L. Nicoud, M. Lattuada, A. Yates, and M. Morbidelli, "Impact of aggregate formation on the viscosity of protein solutions," *Soft Matter* **11**(27), 5513–5522 (2015).
- ⁴⁷R. Pittayanon, J. T. Lau, Y. Yuan, G. I. Leontiadis, F. Tse, M. Surette, and P. Moayyedi, "Gut microbiota in patients with irritable bowel syndrome—A systematic review," *Gastroenterology* **157**(1), 97–108 (2019).
- ⁴⁸A. Tabrizi, L. Khalili, A. Homayouni-Rad, H. Pourjafar, P. Dehghan, and F. Ansari, "Prebiotics, as promising functional food to patients with psychological disorders: A review on mood disorders, sleep, and cognition," *NeuroQuantology* **17**(6), 1–9 (2019).